Decreases in free cholesterol and fatty acid unsaturation in renal cell carcinoma demonstrated by breath-hold magnetic resonance spectroscopy

Rachel Katz-Brull, Neil M. Rofsky, Martina M. Morrin, Ivan Pedrosa, Daniel J. George, M. Dror Michaelson, Robert P. Marquis, Michal Maril, Carolina Noguera and Robert E. Lenkinski

AJP - Renal 288:637-641, 2005. First published Nov 30, 2004; doi:10.1152/ajprenal.00140.2004

AJP - Renal Physiology publishes original manuscripts on a broad range of subjects relating to the kidney, urinary tract, and their respective cells and vasculature, as well as to the control of body fluid volume and composition. It is published 12 times a year (monthly) by the American Physiological Society, 9650 Rockville Pike, Bethesda MD 20814-3991. Copyright © 2005 by the American Physiological Society. ISSN: 0363-6127, ESSN: 1522-1466. Visit our website at http://www.the-aps.org/.

Am J Physiol Renal Physiol 288: F637–F641, 2005.
First published November 30, 2004; doi:10.1152/ajprenal.00140.2004.

Decreases in free cholesterol and fatty acid unsaturation in renal cell carcinoma demonstrated by breath-hold magnetic resonance spectroscopy

Rachel Katz-Brull,[1] Neil M. Rofsky,[1] Martina M. Morrin,[1] Ivan Pedrosa,[1] Daniel J. George,[2] M. Dror Michaelson,[3] Robert P. Marquis,[1] Michal Maril,[1] Carolina Noguera,[1] and Robert E. Lenkinski[1]

[1]*Department of Radiology, Beth Israel Deaconess Medical Center, Harvard Medical School;* [2]*Dana-Farber Cancer Institute, Harvard Medical School; and* [3]*Massachusetts General Hospital, Harvard Medical School, Boston, Massachusetts*

Submitted 19 April 2004; accepted in final form 19 November 2004

Katz-Brull, Rachel, Neil M. Rofsky, Martina M. Morrin, Ivan Pedrosa, Daniel J. George, M. Dror Michaelson, Robert P. Marquis, Michal Maril, Carolina Noguera, and Robert E. Lenkinski. Decreases in free cholesterol and fatty acid unsaturation in renal cell carcinoma demonstrated by breath-hold magnetic resonance spectroscopy. *Am J Physiol Renal Physiol* 288: F637–F641, 2005. First published November 30, 2004; doi:10.1152/ajprenal.00140.2004.— Increased utilization of cross-sectional imaging has resulted in increased detection of incidental renal tumors. The noninvasive characterization of renal tissue has important implications for the diagnosis of renal malignancies and treatment monitoring. Recently, multiple breath-hold averaged proton magnetic resonance spectroscopy (^{1}H-MRS) performed at high field has enabled the use of this noninvasive metabolic profiling technique for the investigation of the abdomen. Multiple breath-hold averaged ^{1}H-MRS at high field (3T) was obtained in the kidneys of 10 healthy volunteers and in renal cell carcinoma tumors of 14 patients. The spectra of normal kidneys showed four main groups of resonances: *1*) at 5.4–5.6 ppm, attributed to C6 of cholesterol and the unsaturated parts of the olefinic region of fatty acids; *2*) at 4.7 ppm, attributed to the residual water signal; *3*) at 3.2 ppm, attributed to trimethylamine moiety of choline metabolites; and *4*) at 1.3 and 0.9 ppm, attributed to the methylenes and terminal methyls of lipids. The ratio of the signal at 5.4 ppm to that of 1.3 ppm was 19-fold lower in renal cell carcinomas than in healthy kidneys, tied $P = 0.0003$ Mann-Whitney *U*-test, suggesting a decrease in both free cholesterol and the degree of unsaturation of fatty acids in the malignant tissue. This metabolic shift is in agreement with previous ex vivo studies of human renal cell carcinoma. The ability to detect renal metabolic shifts noninvasively may improve the specificity of preoperative renal tissue characterization and may provide a new modality for treatment monitoring.

clinical study; proton magnetic resonance spectroscopy; 3T

THE INCREASED USE OF CROSS-SECTIONAL imaging has resulted in the detection of many more tumors at an early stage compared with the era prior to this capacity (23). The crucial feature in characterizing renal masses is in demonstrating the presence or absence of enhancement following the administration of contrast media with either computed tomography (CT) or magnetic resonance imaging (MRI) (14, 20). The demonstration of enhancement indicates a vascular supply and, in effect, excludes simple cysts. However, enhancement can occur in both benign and malignant neoplasms. Given an estimated incidence of renal cell carcinoma (RCC) in the United States at ~31,000 cases/yr, the increased need for characterization of renal masses detected by imaging, and the influx of new therapies under investigation, further refinement for renal mass characterization is needed. Currently, the main role of imaging is to aid in the distinction of enhancing renal masses that require surgical therapy from those that do not. In addition, imaging has an important role in monitoring the response to therapy to aid identification of patients who respond to treatment and those in whom treatment fails.

Symptoms from RCC are generally caused by either local spread of the tumor, causing pain, hematuria, or flank mass, or from the manifestations of distant metastatic spread. Patients with RCC whose tumors are discovered incidentally while still asymptomatic are most likely to be cured (24). About one-third of patients with RCC have metastatic disease at the time of diagnosis. For these patients, the 5-yr survival rate is <10%, and the most beneficial therapeutic course is still under investigation. The success rate of chemotherapy is poor. Nephrectomy of the diseased kidney or a solitary metastasis and radiotherapy have been shown to alleviate some symptoms and pain. Immunotherapy studies with interferon-α, interleukin-2, a combination of these cytokines with 5-fluorouracil, and autolymphocyte therapy have been associated with a response rate of ~6–21% (7, 16, 17, 24, 28, 30). New approaches such as antiangiogenic therapy are currently being investigated extensively in several centers, including our own medical centers (15). Because of the limited response rate to all known treatments, a sensitive assessment of early response to treatment is desirable.

The noninvasive characterization of renal lesions has, therefore, important implications for the diagnosis of renal malignancies and treatment monitoring. Methods to assess tumor response to a variety of treatment regimes have been largely based on the measurements of tumor size. Unlike the tumor response to effective conventional chemotherapy, effective treatment with newer antiangiogenic agents may result in tumor dormancy without tumor shrinkage. As a result, the traditional assessment of any antitumor effect by sequential measurements of tumor size using noninvasive imaging modalities may not be useful in assessing the response to antian-

Address for reprint requests and other correspondence: R. E. Lenkinski, Dept. of Radiology, Beth Israel Deaconess Medical Ctr., 330 Brookline Ave., Boston, MA 02215 (E-mail: rlenkins@bidmc.harvard.edu).

The costs of publication of this article were defrayed in part by the payment of page charges. The article must therefore be hereby marked "*advertisement*" in accordance with 18 U.S.C. Section 1734 solely to indicate this fact.

giogenic treatments. Of the imaging modalities that are commonly used for tumor imaging, dynamic enhanced MRI offers the advantages of high contrast and temporal resolution, lack of ionizing radiation, and excellent soft tissue definition. In addition, the availability of a contrast agent approved for human use (gadolinium-diethylene-triamine pentaacetic acid) that is safe in patients with renal insufficiency is a particular advantage in this group of patients (8, 19, 20). As an adjunct to this modality, proton magnetic resonance spectroscopy (MRS) has been shown to aid in tissue characterization in the brain, breast, and prostate using metabolic markers of malignancy (9, 12, 18, 31).

The purpose of this study was to investigate whether there are metabolic differences between healthy renal tissue and RCC that could be observed in vivo by MRS. A multiple breath-hold strategy was used for the MRS exam in the abdomen, because this method has been shown to improve the spectral resolution and detection of small signals as it markedly decreased the adverse effects of respiratory motion such as out-of-voxel contamination and phase and frequency variations (11).

MATERIALS AND METHODS

End-expiratory breath-hold MRS data were acquired in the kidneys of 10 healthy volunteers (5 men, 5 women, mean age 26 yr, after 4 h of fasting) and in RCC tumors of 14 patients who participated on an IRB-approved phase I trial of a vascular endothelial growth factor receptor inhibitor, PTK787/ZK222584 (Novartis Pharmaceuticals, East Hanover, NJ, and Schering, Berlin, Germany) in patients with metastatic RCC (6). As part of this study, tumor response was monitored by MRI and spectroscopy. This report focuses on the MRS data in patients before initiation of the antiangiogenic treatment.

Eligible patients had metastatic RCC and ≥1 site of measurable or evaluated disease as determined by Southwestern Oncology Group (SWOG) solid tumor response criteria. Other eligibility criteria included age >18 yr, Karnofsky performance status ≥70, adequate hematological and organ function, and a life expectancy ≥3 mo.

The studies were performed on a 3T scanner (Signa LX, General Electric, Waukesha, WI) equipped with a body coil (transmit) and a receive only torso-phased array surface coil (Gore, Newark, DE) as previously described (11). Frame-by-frame single voxel ($2 \times 2 \times 2$ cm^3) point resolved spectroscopy (PRESS) (1) acquisitions were performed using the PRESS-CSI pulse sequence (GE Medical Systems), with an echo time of 144 ms, repetition time of 2,000 ms, spectral width of 5,000 Hz, and 512 points, without outer voxel suppression. The localization pulses have been described elsewhere (13). Crusher gradients of 32-mT/m amplitude and a duration of 4 ms (maximum crusher width) were equally spaced around the 180° pulses with 10-ms spacing. Partial water suppression was achieved using chemical shift-selective (CHESS) pulses, adjusted manually. The signal-to-noise ratio (SNR) of the residual water signal was ~20 in a single scan. Linear shims were used to correct the B_0 inhomogeneity across the investigated voxel. MRS frames were stored and processed individually.

Each breath hold included two dummy scans and eight acquisition frames. Eight sets of single end-expiratory breath-holds (20 s each) were typically acquired per voxel. For the healthy kidneys, the MRS voxel was positioned within the renal parenchyma, using the axial plane, at the level of the hilum of each kidney, to maximize renal tissue within the sample voxel. For the tumors, the MRS voxel was positioned at the center of the tumor. In those patients with RCCs in whom the normal contralateral kidney was visible in the same imaging plane to that of the tumor (or within 4 cm of that imaging plane), MRS data were obtained from the tumor-free contralateral kidney.

Spectral processing was performed using SAGE (Spectra Analysis by General Electric, a commercially available software package, GE Medical Systems). The free induction decays were phase corrected frame by frame, zero filled to 2,048 points, processed with a line broadening of 10 Hz, and Fourier transformed. The eight breath-hold data sets were summed to maximize the SNR. The spectra were visually inspected before summation to verify reproducible water and lipid signal amplitudes and their relative content. Peak amplitude was determined using the peak height in the frequency domain. The noise peak-to-peak amplitude was determined in the frequency domain as well. Noise root mean square (rms) was approximated by dividing the noise peak-to-peak amplitude by 2.8. Of the four data sets, acquired by each of the receiver coils in the phased array coil, the data set with the highest signal-to-noise ratio (nearest to the MRS voxel) was selected for further analysis. The signal-to-noise ratio (peak amplitude divided by the noise rms) of this dataset was standardized to 8 breath holds (64 scans, 2.1 min) and a 6.4-cm distance from the nearest surface coil (of the phased array coil). The signal-to-noise ratio was linearly normalized to the distance of the MRS voxel from the nearest surface coil because, to a first approximation, with the coil size and the anatomic sites investigated here, the reception of a surface coil decreases linearly with the distance from the coil (21). This distance was approximated by determining the shortest anterior-posterior distance from the MRS voxel to the perimeters of the body (using electronic calipers on soft copy MR images), whereas the torso array coil was wrapped around the patient's abdomen.

RESULTS

The MRS study of the kidneys of healthy volunteers utilized abdominal MRI for the selection of the MRS region of interest (MRS voxel). An axial single-shot fast-spin echo (SSFSE) image of the abdomen of one of the volunteers is shown in Fig. 1*A*. The location of the MRS voxel in the kidney is outlined by a white square and marked with an arrow. The average distance of the MRS voxels in the kidneys to the nearest surface coil was 6.4 ± 0.9 cm (n = 20). Figure 1*B* shows a typical breath-hold spectrum of the healthy kidney (voxel shown in Fig. 1*A*). The main observed resonances were at 5.4–5.6 ppm (arrow), attributed to C6 of cholesterol and the unsaturated protons of the olefinic region of fatty acids; 4.7 ppm, attributed to the residual water signal (the peak was cut due to enlargement of the spectrum); 3.2 ppm, attributed to trimethylamine moiety of choline metabolites; 1.3 ppm, attributed to the methylenes of fatty acids, triglycerides, and phospholipids; and ~0.9 ppm, attributed to the terminal methyls of fatty acids, triglycerides, and phospholipids and cholesterol methyls. Resonances at 2.1–2.2 and at 2.5–2.6 ppm, attributed to the methylenes of cholesterol and fatty acids as well as amino acids, were occasionally detected. The expanded chemical shift range of the same spectrum showing the resonance at 5.4 ppm is shown in Fig. 1*C*. The same chemical shift range in a spectrum of another healthy kidney from a different volunteer is shown in Fig. 1*D*. The mean signal-to-noise ratio of the resonances in the healthy kidneys is summarized in Table 1. The signal-to-noise ratio of these resonances was similar in the kidneys on both sides.

The MRS exam was then performed in the RCC tumors, some of which were metastatic tumors. Of the 14 patients evaluated by MRS, the majority (86%) had clear cell carcinoma as their primary tumor type, 36% were women, and the median age was 59 yr. The median number of metastatic sites was two (range, 1–3 sites), and the median number of prior systemic therapies was one.

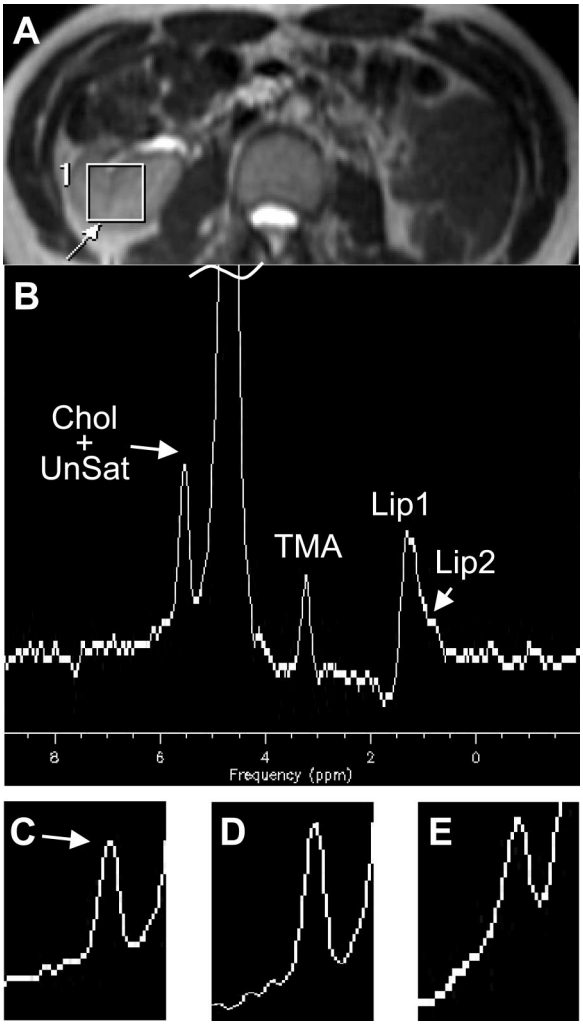

Fig. 1. Magnetic resonance image and spectra of kidneys. *A*: axial single-shot fast-spin echo image of the abdomen of 1 of the healthy volunteers demonstrating the right kidney. The location of the magnetic resonance spectroscopy (MRS) voxel in the kidney is outlined by a white square and marked with an arrow. *B*: typical breath-hold MRS spectrum of the healthy kidney from the voxel shown in *A*. The resonance at 5.4–5.6 ppm was attributed to C6 of cholesterol and the unsaturated parts of the olefinic region of fatty acids (Chol+UnSat). The resonance at 4.7 ppm is due to the residual water signal, and its peak was cut due to magnification of the spectrum. The resonance at 3.2 ppm was attributed to trimethylamine (TMA) moiety of choline metabolites. The resonance at 1.3 ppm was attributed to the methylenes of fatty acids, triglycerides, and phospholipids (Lip1), and the resonance at 0.9 ppm was attributed to the terminal methyls of fatty acids, triglycerides, and phospholipids and cholesterol methyls (Lip2). *C*: expanded chemical shift range (6.5–5 ppm) of the spectrum shown in *B* demonstrating the Chol+UnSat resonance at 5.4 ppm (arrow). *D*: same chemical shift range in a spectrum of a kidney from a different healthy volunteer showing the Chol+UnSat resonance at 5.4 ppm. *E*: same chemical shift range in a spectrum of a tumor-free kidney of a renal cell carcinoma patient, showing a similar Chol+UnSat resonance at 5.4 ppm. The image of this kidney is shown in Fig. 2*A*, and the MRS voxel of this spectrum is outlined by a dotted white line.

Figure 2*A* demonstrates an axial image of the abdomen of one of the patients. The location of the MRS voxel in the center of the RCC tumor is outlined by a solid white line. Figure 2*B* shows the breath-hold spectrum of the tumor that is shown in Fig. 2*A*. Note the presence of prominent resonances at 3.2 and 1.3 ppm and the absence of the resonance at 5.4 ppm. The mean signal-to-noise ratios of the resonances in the tumors are summarized in Table 1. The signal at 5.4 ppm was detected in only 2 of the 14 patients. In addition, in those spectra where this signal was detected there was a large signal at 1.3 ppm, indicating a high lipid concentration in these two MRS voxels. Thus it is conceivable that a large part of the signal at 5.4 ppm that was detected in these two tumors was due, in part, to a large concentration of lipids (and their unsaturated portion) in the voxel. To emphasize the role of cholesterol and unsaturated fatty acids, the ratio of the signal at 5.4 ppm to that of 1.3 ppm was calculated (Table 1). This ratio was found to be 19-fold lower in RCC (tied $P = 0.0003$ on a Mann-Whitney U-test).

To investigate the potential influence of line width variations on the results, the full width at half-height of the signal at 3.2 ppm was determined in the healthy kidneys and the RCC tumors and found to be similar (19.7 ± 4.3 and 18.5 ± 4.6 Hz, respectively).

MRS data were obtained from the tumor-free contralateral kidney in four RCC patients (see MATERIALS AND METHODS). Figure 1*E* demonstrates the MRS spectrum of such a tumor-free kidney in a patient. The spectrum was enlarged to emphasize the signal at 5.4 ppm. This signal was present in all of the unaffected kidneys (4/4) that were investigated. In the other patients, either the kidneys were not disease free or the unaffected renal tissue was outside the MRS sampling plane. In the latter circumstance, the MRS examination of unaffected renal parenchyma would have required either the repositioning the patient and the torso coil or a separate, dedicated MRS evaluation, both pursuits too lengthy for completion of the required protocol.

DISCUSSION

The MRS determination of metabolite concentrations is relative rather than absolute and requires the acquisition of a reference signal. In MRS of the brain, the creatine signal has been found to be close to 10 mM under a variety of conditions and in most brain areas. For this reason, the creatine signal has been used as an internal reference for the determination of concentration in the brain. However, in the breast and prostate none of the MRS signals appears to be detected at a constant level, and therefore these tissues lack an internal reference for MRS examinations. Because of our early stage in the evolution of breath-hold MRS in the abdomen, which enabled the current investigation in the kidney, we have yet to determine whether the spectra of renal tissue contain a signal that can be used as an internal reference. Instead, we used the noise as a basis for comparison between the signals of healthy and malignant tissue. In our experience, the body coil loading was similar from case to case and, as the same voxel size was used throughout the study, the use of signal-to-noise ratios can be justified. The similarity of the full width at half-height of the signal at 3.2 ppm in the healthy kidneys and the RCC tumors suggested that the potential influence of line-width variations on the results was not significant. This result justified the use of peak amplitude as a measure of the signal in the signal-to-noise analysis. This comparison of signal-to-noise ratio was sufficient to establish the significance of the difference between malignant and healthy renal tissue. Moreover, the significance of the difference in the metabolite ratio (5.4-ppm SNR/1.3-ppm SNR), which is, in effect, independent of the noise and the B_0 inhomogeneity, further verified this result. In the future, it may

Table 1. *Signal-to-noise ratio of magnetic resonance signals in healthy kidney and renal cell carcinoma*

	SNR			
	5.4 ppm	3.2 ppm	1.3 ppm	5.4 ppm/1.3 ppm
Healthy kidney (10 volunteers)	7.3±7.4 (10/10 kidneys)	6.8±2.1	30.9±31.7	0.425±0.406 (10/10 kidneys)
Renal cell carcinoma (14 patients)	4.3±14.7† (2/14 tumors)	6.6±8.1	43.1±79.1	0.022±0.056*(2/11 tumors)

Values are means ± SD. SNR, signal-to-noise ratio (MATERIALS AND METHODS). The data from the right kidney of each volunteer are reported. *Statistically significant difference between renal cell carcinoma to healthy kidneys, tied $P = 0.0003$ on Mann-Whitney *U*-test. This analysis included 11 of 14 renal cell carcinoma 5.4-ppm SNR/1.3-ppm SNR values. The other 3 tumors did not show a signal at 1.3 ppm. †Detected in 2 of 14 spectra. The 2 detected SNR values for the 5.4-ppm signal in renal cell carcinoma were 55.1 and 5.6. In the other 12 spectra of renal cell carcinoma, the signal at 5.4 ppm was not detected.

be possible to use an external reference and determine the absolute concentrations of the metabolites that are visible in abdominal MRS.

Previous in vivo proton MRS studies of tissue metabolic profiling have focused on signals in the range of 2–4 ppm, and methods that suppress the spectral regions outside this range have been utilized (22, 25). Here, we show that the signal at 5.4 ppm (of cholesterol and unsaturated fatty acids) may yield important diagnostic information, with added diagnostic value of the signal at 1.3 ppm (of lipids), suggesting that the detection of these signals in the kidney may be beneficial and should not be compromised.

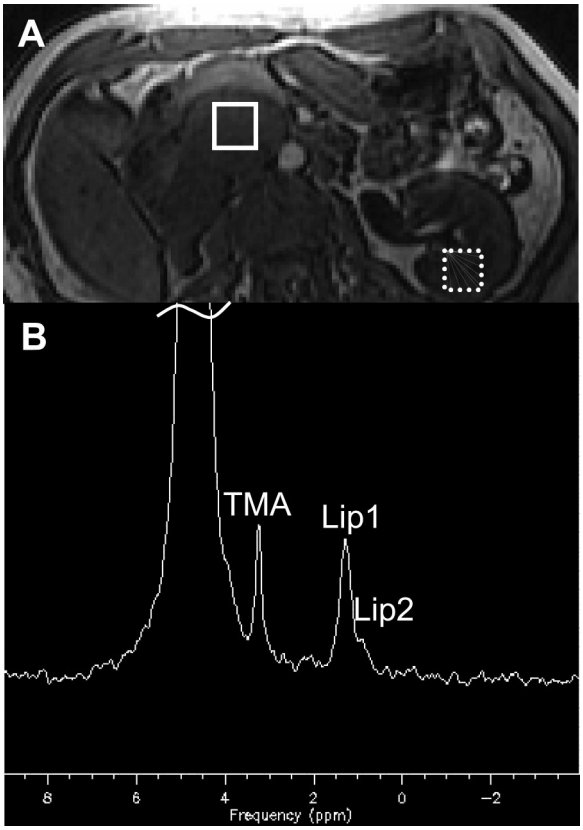

Fig. 2. Magnetic resonance image and spectrum of a renal cell carcinoma. *A*: axial image of the abdomen of 1 of the patients demonstrating the tumor (*right*) and a tumor-free kidney (*left*). The location of the MRS voxel in the tumor is outlined by a solid white line. The location of the MRS voxel in the tumor-free kidney is outlined by a dotted white line, and the spectrum of this voxel is shown in Fig. 1*E*. *B*: typical breath-hold MRS spectrum of the tumor from the voxel in *A*. The resonance at 4.7 ppm is due to the residual water signal, and its peak was cut due to magnification of the spectrum. The resonance at 3.2 ppm was attributed to TMA moiety of choline metabolites. The resonance at 1.3 ppm was attributed to the methylenes of fatty acids, triglycerides, and phospholipids (Lip1), and overlapped the resonance at 0.9 ppm that was attributed to the terminal methyls of fatty acids, triglycerides, and phospholipids and cholesterol methyls (Lip2). Note the absence of resonance at 5.4 ppm.

Partial water suppression enabled the detection of the metabolites while an internal reference for frequency registration was maintained. We did not attempt to reproduce the extent of water suppression from one patient to another. Nevertheless, in the same exam, to ensure that the spectra were recorded from a single region of interest, the spectra were visually inspected before summation to verify reproducible water and lipid signal amplitudes and their relative content.

Excised human renal tissues show more esterified cholesterol and less free cholesterol in RCC compared with healthy kidney tissue, and a decrease in the total unsaturation of the olefinic part of fatty acids was also found in the renal malignancies (29). The resonance at 5.4 ppm has been attributed to cholesterol (specifically in micelles) (5) and to the unsaturated olefinic regions of fatty acids, although the ability to detect cholesterol in the vesicular phases has been debated (3). Either way, the absence of the signal at 5.4 ppm from the in vivo spectra of RCC appears to be in agreement with the previous ex vivo findings. The signal at 5.4 ppm was previously observed in non-breath-hold spectra of the kidneys of healthy volunteers (4); however, it did not appear to be detected in water-soluble extracts of healthy human and bovine kidney (4, 27), suggesting that indeed the molecules that give rise to this signal are lipid soluble. In proton MRS of lipidic extracts (27) of renal tissues and in proton magic angle spinning MRS of intact renal specimens (26), the signal at 5.4 ppm was observed in both healthy and malignant renal tissues. The resonance at 5.4 ppm is due to both esterified cholesterol and free cholesterol. However, the esterified form of cholesterol in RCC specimens was found to be bound to oleate (29), and this large increase in the size of the molecule might limit its detection in vivo, as opposed to its detection in extracts or in magic angle spinning, which would not be affected by oleate binding. Therefore, a decrease in unsaturation of fatty acids and a shift from free cholesterol to bound cholesterol may be the biochemical basis that underlies the absence of the signal at 5.4 ppm in the RCC in vivo spectra.

Because the inclusion of more lipids in the voxel may result in an increase in the concentration of the unsaturated olefinic region and therefore an increase in the signal at 5.4 ppm that is not relevant to the underlying biochemical alterations of the malignant tissues, we calculated the ratio of the 5.4-ppm signal to that of the 1.3-ppm signal (whereas the latter may be correlated with the lipid content in the voxel). This ratio was significantly lower in the RCC, suggesting that this ratio may

be a useful marker for renal malignancy and may potentially aid in monitoring treatment.

Previously, the presence of the signal at 3.2 ppm (attributed to choline metabolites) was found to be a marker of malignancy in the breast (9). Elevation of the magnitude of this signal compared with normal tissue was found in malignant tumors of the brain and prostate (12, 18, 31). In our study, the level of this signal was found to be similar in malignant and healthy renal tissue. However, choline metabolism is tissue specific (10). The kidney has an important role in eliminating excess circulating choline from the body to prevent cholinergic intoxication, and choline metabolites are osmolytes that are important in renal function (2, 32). The results of this study further demonstrate the importance of interpreting pathological metabolic findings in the context of the healthy tissue.

In conclusion, our results suggest that proton MRS may provide additional information to assist in the characterization of renal masses and possibly in the monitoring of new treatment regimens. Further research focusing on the assessment of the sensitivity and specificity of the 5.4 ppm-to-1.3 ppm ratio for renal masses and on the longitudinal MRS evaluation for determining RCC response to therapy is required.

ACKNOWLEDGMENTS

Present address of R. Katz-Brull: Weizmann Institute of Science, Rehovot, Israel.

Present address of D. J. George: Duke Univ. Medical Center, Durham, NC.

REFERENCES

1. **Bottomley PA.** Spatial localization in NMR spectroscopy in vivo. *Ann NY Acad Sci* 508: 333–348, 1987.
2. **Burg MB.** Molecular basis of osmotic regulation. *Am J Physiol Renal Fluid Electrolyte Physiol* 268: F983–F996, 1995.
3. **De Graaf MP, Groen AK, and Bovee WM.** Analysis of micellar and vesicular lecithin and cholesterol in model bile using ^{1}H- and ^{31}P-NMR. *MAGMA* 3: 67–75, 1995.
4. **Dixon RM and Frahm J.** Localized proton MR spectroscopy of the human kidney in vivo by means of short echo time STEAM sequences. *Magn Reson Med* 31: 482–487, 1994.
5. **Ellul JPM, Murphy GM, Parkes HG, Slapa RZ, and Dowling RH.** Nuclear-magnetic-resonance spectroscopy to determine the micellar cholesterol in human bile. *FEBS Lett* 300: 30–32, 1992.
6. **George DJ, Michaelson MD, Oh W, Reitsma D, Laurent D, Mietlowski W, Wang Y, Dugan M, Kaelin WG, and Kantoff P.** Phase I study of PTK787/ZK 222584 in metastatic renal cell carcinoma (Abstract). *Proc Am Soc Clin Oncol* 22: 1548, 2003.
7. **Haas GP, Hillman GG, Redman BG, and Pontes JE.** Immunotherapy of renal-cell carcinoma. *CA Cancer J Clin* 43: 177–187, 1993.
8. **Haustein J, Niendorf HP, Krestin G, Louton T, Schuhmanngiampieri G, Clauss W, and Junge W.** Renal tolerance of gadolinium-DTPA dimeglumine in patients with chronic-renal-failure. *Invest Radiol* 27: 153–156, 1992.
9. **Katz-Brull R, Lavin PT, and Lenkinski RE.** Clinical utility of proton magnetic resonance spectroscopy in characterizing breast lesions. *J Natl Cancer Inst* 94: 1197–1203, 2002.
10. **Katz-Brull R, Margalit R, and Degani H.** Differential routing of choline in implanted breast cancer and normal organs. *Magn Reson Med* 46: 31–38, 2001.
11. **Katz-Brull R, Rofsky NM, and Lenkinski RE.** Breathhold abdominal and thoracic proton MR spectroscopy at 3T. *Magn Reson Med* 50: 461–467, 2003.
12. **Kurhanewicz J, Swanson MG, Nelson SJ, and Vigneron DB.** Combined magnetic resonance imaging and spectroscopic imaging approach to molecular imaging of prostate cancer. *J Magn Reson Imag* 16: 451–463, 2002.
13. **Kurhanewicz J, Vigneron DB, and Nelson SJ.** Three-dimensional magnetic resonance spectroscopic imaging of brain and prostate cancer. *Neoplasia* 2: 166–189, 2000.
14. **Macari M and Bosniak MA.** Delayed CT to evaluate renal masses incidentally discovered at contrast-enhanced CT: demonstration of vascularity with deenhancement. *Radiology* 213: 674–680, 1999.
15. **Morgan B, Thomas AL, Drevs J, Hennig J, Buchert M, Jivan A, Horsfield MA, Mross K, Ball HA, Lee L, Mietlowski W, Fuxius S, Unger C, O'Byrne K, Henry A, Cherryman GR, Laurent D, Dugan M, Marme D, and Steward WP.** Dynamic contrast-enhanced magnetic resonance imaging as a biomarker for the pharmacological response of PTK787/ZK 222584, an inhibitor of the vascular endothelial growth factor receptor tyrosine kinases, in patients with advanced colorectal cancer and liver metastases: results from two phase I studies. *J Clin Oncol* 21: 3955–3964, 2003.
16. **Motzer RJ, Bacik J, Murphy BA, Russo P, and Mazumdar M.** Interferon-α as a comparative treatment for clinical trials of new therapies against advanced renal cell carcinoma. *J Clin Oncol* 20: 289–296, 2002.
17. **Motzer RJ, Murphy BA, Bacik J, Schwartz LH, Nanus DM, Mariani T, Loehrer P, Wilding G, Fairclough DL, Cella D, and Mazumdar M.** Phase III trial of interferon α-2a with or without 13-*cis*-retinoic acid for patients with advanced renal cell carcinoma. *J Clin Oncol* 18: 2972–2980, 2000.
18. **Negendank W.** Studies of human tumors by MRS: a review. *NMR Biomed* 5: 303–324, 1992.
19. **Prince MR, Arnoldus C, and Frisoli JK.** Nephrotoxicity of high-dose gadolinium compared with iodinated contrast. *J Magn Reson Imaging* 6: 162–166, 1996.
20. **Rofsky NM, Weinreb JC, Bosniak MA, Libes RB, and Birnbaum BA.** Renal lesion characterization with gadolinium-enhanced MR imaging: efficacy and safety in patients with renal insufficiency. *Radiology* 180: 85–89, 1991.
21. **Schenck JF, Hart HRJ, Foster TH, Edelstein WA, and Hussain MA.** High resolution magnetic resonance imaging using surface coils. *Magn Reson Annu*: 123–160, 1986.
22. **Schricker AA, Pauly JM, Kurhanewicz J, Swanson MG, and Vigneron DB.** Dualband spectral-spatial RF pulses for prostate MR spectroscopic imaging. *Magn Reson Med* 46: 1079–1087, 2001.
23. **Smith SJ, Bosniak MA, Megibow AJ, Hulnick DH, Horii SC, and Raghavendra BN.** Renal cell carcinoma: earlier discovery and increased detection. *Radiology* 170: 699–703, 1989.
24. **Sokoloff MH, deKernion JB, Figlin RA, and Belldegrun A.** Current management of renal cell carcinoma. *CA Cancer J Clin* 46: 284–302, 1996.
25. **Star-Lack JM, Adalsteinsson E, Gold GE, Ikeda DM, and Spielman DM.** Motion correction and lipid suppression for ^{1}H magnetic resonance spectroscopy. *Magn Reson Med* 43: 325–330, 2000.
26. **Tate AR, Foxall PJ, Holmes E, Moka D, Spraul M, Nicholson JK, and Lindon JC.** Distinction between normal and renal cell carcinoma kidney cortical biopsy samples using pattern recognition of ^{1}H magic angle spinning (MAS) NMR spectra. *NMR Biomed* 13: 64–71, 2000.
27. **Tosi MR, Fini G, Tinti A, Reggiani A, and Tugnoli V.** Molecular characterization of human healthy and neoplastic cerebral and renal tissues by in vitro ^{1}H NMR spectroscopy. *Int J Mol Med* 9: 299–310, 2002.
28. **Tourani JM, Pfister C, Tubiana N, Ouldkaci M, Prevot G, Lucas V, Oudard S, Malet M, Cottu P, Ferrero JM, Mayeur D, Rixe O, Sun XS, Bernard O, Andre T, Tournigand C, Muracciole X, and Guilhot J.** Subcutaneous interleukin-2 and interferon alfa administration in patients with metastatic renal cell carcinoma: final results of SCAPP III, a large, multicenter, phase II, nonrandomized study with sequential analysis design–the subcutaneous administration propeukin program cooperative group. *J Clin Oncol* 21: 3987–3994, 2003.
29. **Tugnoli V, Bottura G, Fini G, Reggiani A, Tinti A, Trinchero A, and Tosi MR.** H-1-NMR and C-13-NMR lipid profiles of human renal tissues. *Biopolymers* 72: 86–95, 2003.
30. **Yang JC, Sherry RM, Steinberg SM, Topalian SL, Schwartzentruber DJ, Hwu P, Seipp CA, Rogers-Freezer L, Morton KE, White DE, Liewehr DJ, Merino MJ, and Rosenberg SA.** Randomized study of high-dose and low-dose interleukin-2 in patients with metastatic renal cancer. *J Clin Oncol* 21: 3127–3132, 2003.
31. **Zakian KL, Eberhardt S, Hricak H, Shukla-Dave A, Kleinman S, Muruganandham M, Sircar K, Kattan MW, Reuter VE, Scardino PT, and Koutcher JA.** Transition zone prostate cancer: metabolic characteristics at H-1 MR spectroscopic imaging. Initial results. *Radiology* 229: 241–247, 2003.
32. **Zeisel SH and Blusztajn JK.** Choline and human nutrition. *Annu Rev Nutr* 14: 269–296, 1994.